Structure and dynamics of hexafluoroisopropanol-water mixtures by x-ray diffraction, small-angle neutron scattering, NMR spectroscopy, and mass spectrometry

Koji Yoshida and Toshio Yamaguchi[a)]
Department of Chemistry, Faculty of Science, Fukuoka University, Nanakuma, Jonan-ku, Fukuoka, 814-0180, Japan

Tomohiro Adachi and Toshiya Otomo
Institute for Materials Structure Science, High Energy Accelerator Research Organization (KEK), Oho, Tsukuba 305-0801, Japan

Daisuke Matsuo and Toshiyuki Takamuku
Department of Chemistry, Faculty of Science and Engineering, Saga University, Honjo-machi, Saga 840-8502, Japan

Nobuyuki Nishi
Institute for Molecular Science, Myodaiji, Okazaki, 444-8585, Japan

(Received 25 February 2003; accepted 26 June 2003)

The structure and dynamic properties of aqueous mixtures of 1,1,1,3,3,3-hexafluoro-2-propanol (HFIP) have been investigated over the whole range of HFIP mole fraction (x_{HFIP}) by large-angle x-ray scattering (LAXS), small-angle reutron scattering (SANS), ^{19}F-, ^{13}C-, and ^{17}O-NMR chemical shifts, ^{17}O-NMR relaxation, and mass spectrometry. The LAXS data have shown that structural transition of solvent clusters takes place at $x_{\mathrm{HFIP}}\sim 0.1$ from the tetrahedral-like hydrogen bonded network of water at $x_{\mathrm{HFIP}}\lesssim\sim 0.1$ to the structure of neat HFIP gradually formed with increasing HFIP concentration in the range of $x_{\mathrm{HFIP}}\gtrsim 0.15$. The Ornstein–Zernike plots of the SANS data have revealed a mesoscopic structural feature that the concentration fluctuations become largest at $x_{\mathrm{HFIP}}\sim 0.06$ with a correlation length of ~ 9 Å, i.e., maximum in clustering and microhetrogeneities. The ^{19}F and ^{13}C chemical shifts of both CF_3 and CH groups of HFIP against x_{HFIP} have shown an inflection point at $x_{\mathrm{HFIP}}\sim 0.08$, implying that the environment of HFIP molecules changes due to the structural transition of HFIP clusters. The ^{17}O relaxation data of water have shown that the rotational motion of water molecules is retarded rapidly upon addition of HFIP into water up to $x_{\mathrm{HFIP}}\sim 0.1$, moderately in the range of $\sim 0.1<x_{\mathrm{HFIP}}\lesssim 0.3$, and almost constant at $x_{\mathrm{HFIP}}\gtrsim 0.3$, reflecting the structural change in the solvent clusters at $x_{\mathrm{HFIP}}\sim 0.1$. The mass spectra of cluster fragments generated in vacuum from HFIP-water mixtures have shown that the predominant clusters are A_1W_n ($n<12$, $A=$HFIP, $W=$water) and water clusters W_n ($n=5-8$) at $x_{\mathrm{HFIP}}=0.09$ and 0.20 and only HFIP oligomers in a water-rich region of $x_{\mathrm{HFIP}}=0.005\sim 0.01$. From all the information obtained in the present study, the models are proposed for the aggregation of HFIP and water molecules in HFIP-water mixtures. © *2003 American Institute of Physics.* [DOI: 10.1063/1.1602070]

I. INTRODUCTION

Alcohol-water binary solutions have recently been revisited in the biophysics and biochemistry fields due to their importance in understanding phenomena, such as the alcohol-induced α-helix promotion of peptides and proteins in aqueous solution.[1–12] Among various alcohols available, fluoroalcohols, such as 2,2,2-trifluoroethanol (TFE) and HFIP, have been found to be more effective than aliphatic alcohols in stabilizing the α-helical structure of peptides and proteins;[6–12] e.g., HFIP has been found to be about 20 times more effective than methanol in the denaturation of β-lactoglobulin and the helix formation of melittin.[12]

In recent years, an advanced x-ray diffraction technique with an imaging plate as an area detector and neutron diffraction with isotopic substitution method combined with molecular simulation (empirical potential structure refinement) have enabled us to determine the detailed structure of aqueous mixtures of methanol,[13] ethanol,[14–16] and *tert*-butanol[17] as a function of alcohol concentration at a molecular level. Mass spectrometry has also been proved to be useful for estimating the composition of solvent clusters of alcohol-water mixtures.[13–16] The results of these studies have demonstrated that structural transition of solvent clusters takes place at specific alcohol concentrations depending on the nature of the hydrophobic groups of alcohols. Interestingly the specific alcohol concentrations of the structural transition are consistent with those where anomalies in various physicochemical properties are observed for alcohol-water binary solutions. Furthermore, our previous circular dichroism (CD) spectral measurements of chymotrypsin in-

a)Author to whom correspondence should be addressed. Electronic mail: yamaguch@fukuoka-u.ac.jp; Fax: +81-92-865-6030.

hibitor 2 in ethanol-water mixtures[18] have shown an inflection point in the transformation from β-sheets to α-helix structure near the structure transition concentration, implying that solvent clusters play an important role in the change of the secondary structure of peptides and the denaturation of proteins in aqueous solution.

Thus, the microscopic structure and dynamic properties of clusters formed in HFIP-water binary solutions are essential for understanding the physicochemical properties of aqueous HFIP mixtures and their strong α-helix stabilization of peptides and proteins. The hydration of fluorocarbons in aqueous solution is usually accompanied by a negative change of enthalpy and entropy, and their magnitudes are larger than those for the corresponding hydrocarbons with the same number of carbon atoms.[19] So far, the structure of HFIP-water mixtures has been investigated by molecular dynamics simulation on an infinitely dilute system of 216 water molecules and one HFIP molecule.[20] The results showed that the hydrogen bonding is enhanced around the hydroxyl group. However, clustering in HFIP molecules was not examined. Raman spectra and ^{13}C NMR spectra were measured for HFIP-water mixtures over the whole range of HFIP concentration, suggesting the formation of micelle-like assemblies with the fluoroalkyl groups as an inside core, although its structural details remain unexplored.[21] Very recently, a molecular dynamics simulation study on HFIP-water mixtures over a whole range of HFIP mole fractions has been reported.[22] Although simulated thermodynamic properties of pure HFIP are in good agreement with the experimental data, the model potentials failed to reproduce the mixing enthalpy for the mixtures. In order to validate the simulation and improve the pair potentials of HFIP-water mixtures, experimental data such as the structure factors and the radial distribution functions, which can be compared directly with those obtained by the simulation, are highly needed. Hong *et al.* have performed small-angle x-ray scattering of aqueous HFIP solutions and found that maximum aggregation of HFIP molecules occurs at around 30%(v/v) HFIP or $x_{\mathrm{HFIP}} = 0.0671$.[23] Furthermore, from their CD study on conformational transition of melittin and β-lactoglobulin induced by HFIP against the extent of cluster formation, they have suggested that clustering of alcohol molecules is an important factor to enhance the effects of alcohols on proteins and peptides.

In the present study, we have performed large-angle x-ray diffraction (LAXS), small-angle neutron scattering (SANS), ^{19}F-, ^{13}C-, and ^{17}O-NMR chemical shifts, ^{17}O-NMR relaxation, and mass spectroscopy measurements and revealed the structure of predominant solvent clusters in HFIP-water mixtures at a molecular level from the microscopic to mesoscopic ranges, the composition and size of the clusters, and the dynamic properties of water molecules as a function of HFIP mole fraction.

Section II describes the details of various experiments employed. In Sec. III we present experimental radial distribution functions, the concentration fluctuations and size of the clusters, the rotational motions of water molecules in the aqueous HFIP mixtures, and the composition of the clusters. Section IV summarizes the results and concludes the most likely model of the solvent clusters in aqueous HFIP mixtures.

II. EXPERIMENT

A. Preparation of samples

HFIP (Wako Pure Chemicals, extra grade) was used without further purification. HFIP and doubly distilled water were weighed to the required compositions of the sample solutions used for x-ray diffraction measurements. For the SANS measurements, D_2O (Aldrich, D content 99.8%) was used instead of light water without further purification and mixed with HFIP. The densities of the sample solutions were determined at 25 °C with a densimeter (Anton Paar K.G. DMA 48). For the NMR measurements, $H_2\,^{17}O$ (CDN, 27 at.% ^{17}O) was diluted by adding doubly distilled water to the atomic fractions of ^{17}O enough to obtain a good signal to noise ratio and then mixed with HFIP to the required concentrations.

B. X-ray diffraction

X-ray diffraction measurements were made at room temperature on HFIP-water mixtures over the whole mole fraction range of HFIP including pure water and HFIP ($0 \leqslant x_{\mathrm{HFIP}} \leqslant 1$). A rapid liquid x-ray diffractometer (BRUKER AXS, DIP301), combined with an imaging plate (Fuji Film Co. Ltd.) as a two-dimensional detector, was used for all measurements. Details of the diffractometer and its performance have been described elsewhere.[24,25] X-rays were generated by a rotary Mo anode (Rigaku, RU-300) operated at 50 kV and 200 mA, and then monochromatized by a flat graphite crystal to obtain Mo $K\alpha$ radiation (the mean wavelength $\lambda = 0.7107$ Å). A sample solution sealed in a glass capillary (W. Müller, i.d. 2.00 mm, o.d. 2.02 mm) was exposed to x-rays for 1 h. An empty glass capillary was also measured in order to correct for the cell scattering. The observed range of the scattering angle (2θ) was 0.1 to 109°, corresponding to a scattering vector $s(=4\pi\lambda^{-1}\sin\theta)$ of 0.02 to 14.4 $\mathrm{Å}^{-1}$.

The two-dimensional x-ray intensities, $I_{obs}(x,y)$, accumulated on the imaging plate were corrected for polarization and then integrated into one-dimensional data, $I_{obs}(\theta)$, as described previously.[24–26] The experimental intensities for the sample and the empty capillary were corrected for absorption.[24,25] The intensity of the empty capillary was then subtracted in order to extract the contribution from the sample solution alone. The corrected intensities were normalized to electron units by conventional methods.[27–29] The contribution of the incoherent scattering, $I^{inco}(s) = \Sigma x_i I_i^{inco}(s)$, was subtracted from the normalized intensities to obtain the coherent scattering intensity, $I^{coh}(s)$, where x_i is the number of atoms i in a stoichiometric volume V per O atom of water and/or HFIP molecules, and $I_i^{inco}(s)$ is the Compton scattering intensity of atoms i.[30] The structure function, $i(s)$, is given by

$$i(s) = I^{coh}(s) - \Sigma x_i f_i^2(s), \tag{1}$$

TABLE I. Intramolecular parameter values (Ref. 20) used in the calculations. r_{ij}, n_{ij}, and b_{ij} are the interatomic distance, number of interactions, and temperature factor in Eq. (3), respectively.

	r_{ij}/Å	n_{ij}	b_{ij}/Å^2
HFIP			
O–H	0.992	1	0.005
C_2–H	1.095	1	0.005
F_1–C_1, F_2–C_3	1.371	6	0.005
C_2–O	1.428	1	0.005
(C_1,C_3)–C_2	1.558	2	0.005
F_1–F_1, F_2–F_2	2.150	6	0.005
(F_1,F_2)–C_2	2.393	6	0.005
(C_1,C_3)–O	2.442	2	0.005
H_2O			
O–H	0.970	2	0.002
H–H	1.555	1	0.010

where $f_i(s)$ represents the scattering factor of atom i corrected for anomalous dispersion.[31] The s-weighted structure function was Fourier transformed into the radial distribution function (RDF), $G(r)$, as

$$G(r)=1+\frac{1}{2\pi^2 r\rho_0}\int_{s\,\min}^{s\,\max} si(s)M(s)\sin(rs)ds. \qquad (2)$$

Here, ρ_0 is the number density of a sample solution, $s_{\min}$ and $s_{\max}$ are the minimum and maximum s-values, respectively, attained in the measurements. A modification function, $M(s)$, of the form $[\Sigma x_i f_i(s)]^{-2}\exp(-0.01s^2)$ was used to correct the phase shift of electrons and to minimize the termination effect caused by finite Fourier transformation.

The contribution of the intramolecular interactions within HFIP and water molecules, which are characterized by the interatomic distance r_{ij}, the temperature factor b_{ij}, and the number of interactions n_{ij} for each atom pair i-j, was calculated by Eq. (3)

$$i_{intra}(s)=\sum_i \sum_j n_{ij}f_i(s)f_j(s)\frac{\sin(r_{ij}s)}{r_{ij}s}\exp(-b_{ij}s^2), \qquad (3)$$

and subtracted from the observed structure function, $i(s)$, to derive the differential structure function, $i_{diff}(s)$, which includes the intermolecular interactions as well as a part of intramolecular contribution not taken into account. The values of the intramolecular parameters r_{ij} and n_{ij} of HFIP and H_2O were cited from the literature[20] and are summarized in Table I, together with the b_{ij} values experimentally estimated to obtain a good fit to the experimental RDFs. The intramolecular distances over 2.6 Å within an HFIP molecule vary depending on the conformation of both of the terminal CF_3 groups and thus their contributions were not taken into account in the above calculations. The corresponding difference RDF (DRDF) was calculated by Fourier transformation of $i_{diff}(s)$ with Eq. (2). All the treatments of the x-ray diffraction data were carried out with the program KURVLR.[26]

C. Small-angle neutron scattering

The scattering lengths of H and D for neutrons have a contrast of -3.74 and 6.67 fm, respectively,[32] and hence when D_2O is used as a solvent instead of H_2O, the aggregation or concentration fluctuations in the HFIP-water binary mixtures have a good contrast in SANS (which is thus superior to SAXS, small-angle x-ray scattering). In the HFIP-D_2O binary mixtures the hydroxyl D and H atoms within D_2O and HFIP may exchange, but the aggregation or concentration fluctuations still show good contrast because of the much higher D_2O concentration at the mole fractions investigated.

SANS measurements were made at two different facilities. In the first run the HFIP-D_2O mixtures at $x_{\mathrm{HFIP}}=0.045$, 0.089, and 0.134 were measured on the small-angle neutron spectrometer WINK at the spallation neutron facility (KENS) of the National Laboratory for High Energy Accelerator Research Organization (KEK). The wavelengths of cold neutrons used were 1–16 Å, corresponding to the scattering vector range 0.01–10 Å^{-1}. The neutron beam size at the sample position was 20 mm×20 mm. A sample solution was inserted in a rectangular quartz cell of 22 mm in width, 40 mm in height, and 2 mm in sample thickness. The accumulated time was 6–7 h per sample.

The second measurements were made for the HFIP-D_2O mixtures at $x_{\mathrm{HFIP}}=0.0305$, 0.0427, 0.0710, 0.106, and 0.152 on the small-angle spectrometer SANS-U at the reactor JRR-3M in the Japan Atomic Energy Research Institute (JAERI). The wavelength used was 6 Å. The neutron beam size at the sample position was 7 mm ϕ. A sample was kept in a quartz cell of 2 mm path length. A typical accumulated time was 1 h per sample. Measurements were also made for background, an empty cell, and lupolen.

The SANS data of the sample solutions and the empty cell were corrected for absorption by using transmission data measured, and then the empty cell data were subtracted as background. Correction for the detector efficiency and data normalization were made by using the data of H_2O in a quartz cell of 1 mm sample thickness for the WINK data and those of luporen for the SANS-U data. The contribution of the incoherent scattering was then removed from the normalized intensity. The coherent and incoherent scattering lengths of atoms were taken from the literature.[32]

D. ^{19}F-, ^{13}C-, and ^{17}O-NMR measurements

HFIP-H_2O binary solutions were inserted into sample tubes (Pyrex glass) of 10, 5, and 5 mm in diameter without degassing for ^{19}F-, ^{13}C-, and ^{17}O-NMR measurements, respectively. The ^{19}F chemical shift (^{19}F-δ) of the HFIP CF_3 groups in HFIP-water mixtures was measured on an FT-NMR Lamda-500 (JEOL) spectrometer. The ^{13}C chemical shifts (^{13}C-δ) of the HFIP CF_3 and CH groups, ^{17}O chemical shift (^{17}O-δ) and ^{17}O spin-lattice relaxation time (T_1) of H_2 ^{17}O in HFIP-water mixtures were measured on an FT-NMR GSX-400 (JEOL) spectrometer. The FID signals accumulated were 256 for ^{17}O and 256–2048 for ^{13}C depending on HFIP concentration. The signal for ^{19}F was not accumulated. The observed frequency ranges were 54, 20, and 5 kHz, the sampling points were 65 536, 32 768, and 4096, and the frequency resolutions were 1.6 Hz (0.003 ppm), 1.22 Hz (0.012 ppm), and 2.44 Hz (0.04 ppm) for ^{19}F, ^{13}C, and ^{17}O,

respectively. The external reference for ^{13}C-δ was the methyl ^{13}C of sodium 3-(trimethylsilyl)propanesulfonate (TMSP) in D_2O, which was injected into an inner Pyrex glass tube (i.d. 3 mm) placed in an outer tube (i.d. 5 mm). The external reference for ^{19}F-δ was hexafluorobenzene filled in a space between outer and inner coaxial cells (Shigemi, SC-002). The ^{17}O-spin-lattice relaxation time (T_1) was measured by the inversion-recovery method. The number of the delay time τ in the series of $(\pi-\tau-\pi/2)_n$ was 20. The longest delay time exceeded $5T_1$. The experimental errors in T_1 were within $\pm 0.5\%$.

The observed chemical shifts were corrected for the volume magnetic susceptibilities of HFIP-water mixtures by an external double reference method[33–35] described as Eq. (4),

$$\Delta\delta_{\mathrm{CHCl3}} = k\{\chi_S - \chi_{\mathrm{CHCl3}}\}\times 10^6, \tag{4}$$

where k is the shape factor, χ_S and χ_{CHCl3} are the magnetic susceptibilities of solvents and chloroform, respectively.

A capillary (i.d. 1 mm) with a spherical end (o.d. 4 mm) (Shigemi, SSP-51) was placed in an outer capillary (i.d. 4.2 mm). First, the shape factor k of the inner capillary was determined in the following manner. Chloroform was inserted in the inner cell, while the outer cell was filled with water, methanol, ethanol, or acetone of known magnetic susceptibilities. The shape factor k was obtained from the slope of plots of the differences in the two ^1H chemical shifts, $\Delta\delta_{\mathrm{CHCl3}}$, measured for the various solvents against the differences in the magnetic susceptibilities, $\chi_S - \chi_{\mathrm{CHCl3}}$, by Eq. (4).

Next, HFIP-water sample solutions were inserted into the outer cell, and the $\Delta\delta_{\mathrm{CHCl3}}$ values were measured as previously. The χ_S values for the HFIP-water mixtures were calculated from Eq. (4) by using the shape factor obtained above. Those for the external references (TMSP in D_2O and hexafluorobenzene) were also calculated in a similar manner.

The correction of the magnetic susceptibilities was then applied to the chemical shifts, δ_{obs}, for ^{19}F, ^{13}C, and ^{17}O, which had been measured with a cylindrical double tube, according to Eq. (5),

$$\delta_{cor} = \delta_{obs} - (4\pi/3)\{\chi_S - \chi_R\}\times 10^6, \tag{5}$$

where a factor of $4\pi/3$ is the shape factor for the cylindrical double tube and χ_R the magnetic susceptibility of the external references.

The probe temperature was monitored with a thermocouple placed just below the sample tube and controlled to within ± 0.1 °C by passing temperature-controlled air into the probe. The ^{13}C-δ and ^{17}O T_1 values were measured at 30 °C. The ^{17}O T_1 values were also measured at 10 and 30 °C for HFIP-D_2O solutions in a region of $x_{\mathrm{HFIP}} \leqq 0.02$ to estimate temperature dependence of the NMR B coefficient,[36] which gives us the structure information of the hydration shell of an HFIP molecule.

E. Mass spectrometry

HFIP-water mixtures at $x_{\mathrm{HFIP}} = 0.005$, 0.01, 0.09, and 0.20 were measured by mass spectrometry, in which the method of adiabatic expansion of liquid droplets in vacuum was employed as described in detail elsewhere.[37–40] A droplet flow was generated by hydrodynamic conversion of liquid stream from a small notched nozzle of diameter ~40 μm. These droplets were introduced into the high vacuum chambers through two skimmers. We used two different mass spectrometers: a quadrupole mass spectrometer (Extrel 7-162-8 coupled with 311-12H) and a double focus spectrometer with electric and magnetic sectors (Kratos Analytical, Profile). The ionizer of the latter system was modified with a homemade ion repeller. The mass number (m/z) range measured was from 170 to 980. The average temperature of the liquid droplets was estimated to be 40 °C from the temperature-dependent mass spectra of an aqueous solution of propionic acid with an acid mole fraction of 0.005 as previously described.[37,38]

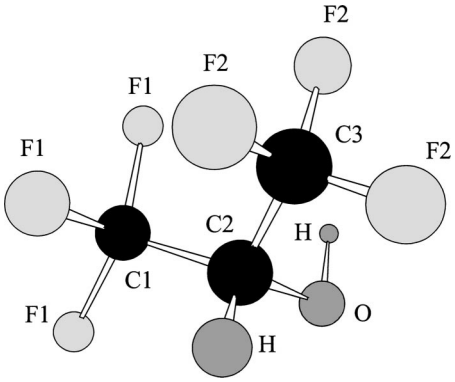

FIG. 1. Molecular structure of HFIP with notation of the atoms.

In our previous studies of aqueous mixtures of methanol,[13] ethanol,[14–16] and dioxane[41] by LAXS and mass spectrometry, the solvent clusters detected on the mass spectra were in good agreement with the short-range ordering revealed by x-ray diffraction of the corresponding bulk solutions, although the adiabatic expansion in vacuum and ionization processes are involved in generating the cluster fragments from the liquid droplets. Thus, the present mass spectra of liquid droplets of HFIP-water mixtures will give us hints of predominant solvent clusters formed in the bulk solutions.

III. RESULTS AND DISCUSSION

A. X-ray structure functions and radial distribution functions

Figure 1 shows the structure of an HFIP molecule with atomic labels, and the intramolecular parameter values are given in Table I. Figure 2 shows the s-weighted structure functions, $i(s)$, for water, HFIP, and their mixtures as a function of HFIP mole fraction. As is seen in Fig. 2, the structure function of pure water ($x_{\mathrm{HFIP}} = 0$) is characterized with two typical peaks observed at 2 and 3 Å^{-1}, which arise from the tetrahedral-like water structure.[24] On the other hand, the structure function for pure HFIP ($x_{\mathrm{HFIP}} = 1$) has a sharp peak at 1.2 Å^{-1} and a broad second peak centered at 3 Å^{-1}. Upon addition of HFIP into water the peak at 1.2 Å^{-1} is gradually enhanced, whereas that at 2 Å^{-1} is decreased. Apparently, in

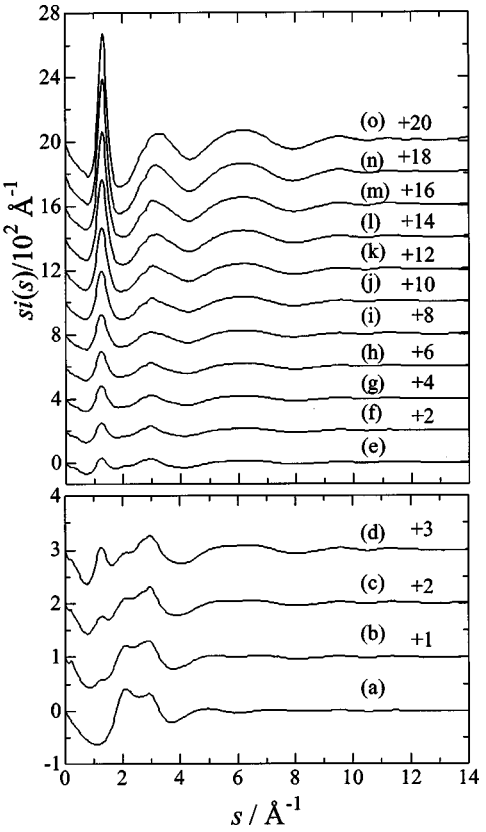

FIG. 2. X-ray *s*-weighted structure functions, $i(s)$, for the HFIP-water mixtures as a function of HFIP mole fraction x_{HFIP} of (a) 0, (b) 0.06, (c) 0.10, (d) 0.15, (e) 0.20, (f) 0.25, (g) 0.30, (h) 0.35, (i) 0.40, (j) 0.50, (k) 0.60, (l) 0.70, (m) 0.80, (n) 0.90, and (o) 1. It should be noted that the structure functions at $x_{\mathrm{HFIP}}=0-0.15$ are magnified by four for clarity, compared with those at $x_{\mathrm{HFIP}}=0.2-1$.

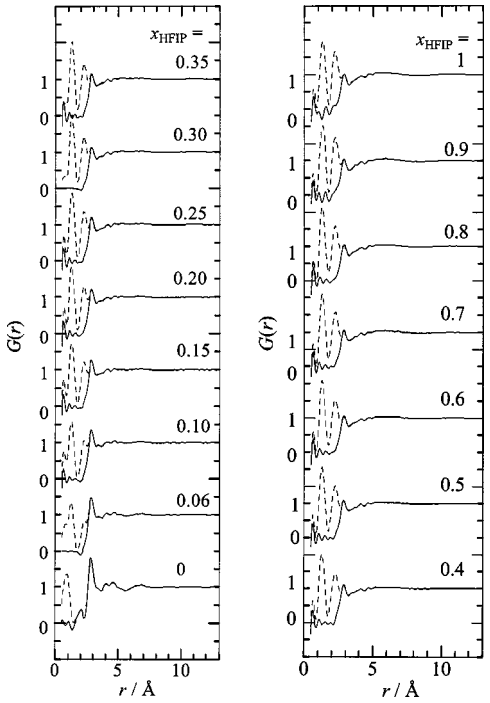

FIG. 3. X-ray radial distribution functions for the HFIP-water mixtures as a function of HFIP mole fraction, x_{HFIP}. The dashed lines show the RDFs obtained from Fourier transform of the values in Fig. 2, whereas the solid lines are difference radial distribution functions (DRDFs) obtained by subtraction of the contribution of the intramolecular interactions within HFIP and water molecules given in Table I, from the total RDFs.

the region of $x_{\mathrm{HFIP}}\leqslant 0.1$ the tetrahedral-like water structure is predominant, but in the range of $0.15\leqslant x_{\mathrm{HFIP}}$ the structure of neat HFIP gradually become important.

Figure 3 shows the corresponding total and differential radial distribution functions, RDFs (dashed lines) and DRDFs (solid lines), respectively. In the DRDF of pure water three dominant peaks are observed at 2.8, 4.5, and 7.0 Å, corresponding to the first-, second-, and third-neighbor O–O interactions, respectively, in the tetrahedral-like hydrogen-bonded network of water.[24] On the other hand, the RDF for pure HFIP has two distinct peaks at 1.4 and 2.3 Å, assigned to the intramolecular interactions given in Table I. The third peak at 2.8 Å consists of the intramolecular F–F interactions within an HFIP molecule and possible O–O hydrogen bonds between HFIP molecules.[22] The broad peaks centered at ~5 and ~10 Å correspond to the first- and second-neighbor intermolecular interactions of HFIP, which are a weighted sum of all atom pairs in HFIP-water mixtures. A similar long-range structure has been reported as peaks at 4.3, 5.0–8.8, and 11 Å in the $g(r)$ of Cc–Cc interactions (Cc denotes the central C atom in an HFIP molecule) from the MD simulation of pure HFIP.[22]

For the HFIP-water mixtures, the three characteristic peaks at 2.8, 4.5, and 7 Å due to the tetrahedral-like water structure are clearly seen at $x_{\mathrm{HFIP}}=0.06$ and 0.10 and less discernible at $x_{\mathrm{HFIP}}=0.15$. In the region of $x_{\mathrm{HFIP}}\geqslant 0.2$ the whole features of DRDFs are very similar to that for pure HFIP, though the amplitudes of the intermolecular peaks at ~5 and ~10 Å increase with increasing HFIP concentration. In the MD study on HFIP-water mixtures the relative positions of the Cc–Cc peaks remain unchanged at 4.3 and 5.0–8.8 Å, but the running integration number of the $g(r)$ (Cc–Cc) at 9 Å does not increase linearly with the HFIP concentration and has an inflection point at 0.34%(v/v) and $x_{\mathrm{HFIP}}=0.082$, which is evidence of cluster formation.[22] The present findings in the $si(s)$ and DRDFs values and the MD results[22] suggest two regimes of predominant solvent clusters with structural transition at $x_{\mathrm{HFIP}}\sim 0.1$:(1)$0\leqq x_{\mathrm{HFIP}}\leqq 0.1$, where the tetrahedral-like structure of water dominates with clustering of HFIP molecules and (2) $0.15\leqq x_{\mathrm{HFIP}}\leqq 1$, where the intrinsic structure of HFIP is gradually enhanced, accompanied by rupturing water structure with increasing x_{HFIP}.

Further detailed analysis of the structure of HFIP-water mixtures has to be waited until neutron diffraction measurement with isotopic substitution and subsequent EPSR simulation are made, which will give us a full set of partial structure factors and radial distribution functions of HFIP-water mixtures.

B. Small-angle neutron scattering

Figure 4 shows the SANS intensities of the HFIP-D_2O mixtures after correction for the incoherent scattering. In order to estimate the concentration fluctuations in the HFIP-D_2O mixtures, Ornstein–Zernike[42] plots were made according to

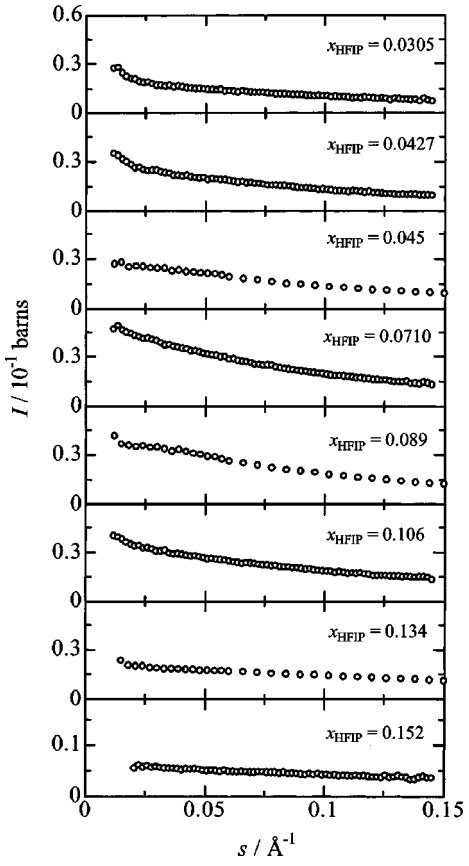

FIG. 4. Normalized SANS intensities, $I(s)$, for the HFIP-D_2O mixtures at various HFIP mole fractions, x_{HFIP}.

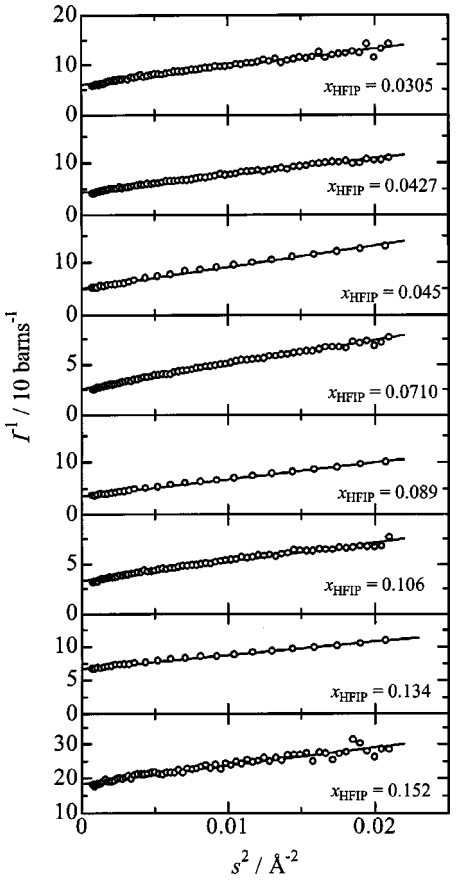

FIG. 5. Ornstein–Zernike plots of the SANS data for the HFIP-D_2O mixtures at various HFIP mole fractions, x_{HFIP}. The circles show the experimental values and the solid lines the fits.

$$I(s)^{-1} = I(0)^{-1}\{1 + \xi^2 s^2\}, \tag{6}$$

where ξ is the Debye correlation length. The correlation lengths were obtained from a least-squares fitting procedure using Eq. (6). The results of the fits are shown in Fig. 5, where the observed values are well reproduced by the fits. The finally optimized ξ values are given in Table II. Figure 6 shows the correlation length against x_{HFIP}. As is seen in Fig. 6, the concentration fluctuations or clusterings in the HFIP-water mixtures have a maximum with a correlation length of 9.7 Å at $x_{HFIP} \sim 0.06$, which is in excellent agreement with that of the previous SAXS data.[23] The maximum concentration fluctuations correspond to the largest microheterogeneities in the HFIP-water mixtures. Since in the present HFIP-D_2O system the hydrophobic CF_3 groups have a good contrast with the solvent D_2O, the present results suggest that with increasing x_{HFIP} up to ~ 0.06 the hydrophobic CF_3 groups of HFIP molecules tend to aggregate, whereas the polar OH groups form hydrogen bonds with surrounding D_2O molecules, and that in the region of $x_{HFIP} \gtrsim 0.06$ the HFIP aggregates are gradually broken to develop the neat HFIP structure.

It is interesting to note that a maximum in the concentration fluctuations of aqueous mixtures of *tert*-butanol of similar bulkiness has been observed at a similar alcohol mole fraction (0.107).[43]

C. ^{19}F and ^{13}C chemical shifts

Figures 7(a), 7(b), and 7(c) show the ^{19}F and ^{13}C chemical shifts of the CF_3 and CH groups, abbreviated as ^{19}F-δ_{CF3}, ^{13}C-δ_{CF3}, and ^{13}C-δ_{CH}, respectively, with and without the correction for the magnetic susceptibility in HFIP-water mixtures against the HFIP mole fraction.

The ^{19}Fδ_{CF3} data, which would give us direct information of the aggregation of HFIP molecules in the mixtures, shifts moderately to a lower-field with decreasing x_{HFIP} from 1 to ~ 0.08 and then does sharply to $x_{HFIP} = 0$, giving rise to an inflection point at $x_{HFIP} \sim 0.08$; the result suggests transition of the coordination environment around the CF_3 groups at $x_{HFIP} \sim 0.08$. The low-field shift or increase in ^{19}F-δ_{CF3}

TABLE II. The correlation lengths ξ as a function of HFIP mole fraction x_{HFIP} obtained from the SANS measurements.

x_{HFIP}	ξ/Å
0.0305	7.73±0.11
0.0427	8.76±0.08
0.0450	8.59±0.09
0.0710	9.66±0.07
0.0890	9.10±0.09
0.106	7.54±0.08
0.134	5.85±0.09
0.152	5.37±0.10

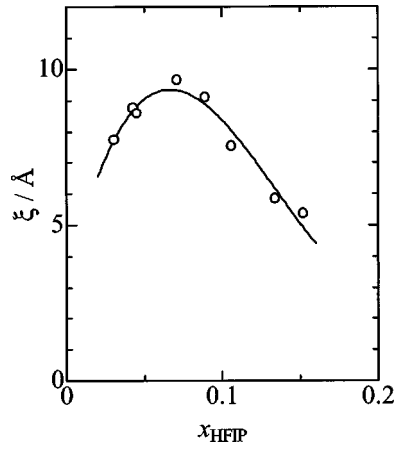

FIG. 6. Correlation lengths ξ against the HFIP mole fraction, x_{HFIP}, for the HFIP-D_2O mixtures. The solid line shows a polynomial least-square fit.

corresponds to a decrease in the electron density of C–F fluorine, i.e., the electrons on the F atoms transfer in part into the C–F bonds. This would be caused by dispersion force induced among the hydrophobic CF_3 groups when they aggregate.

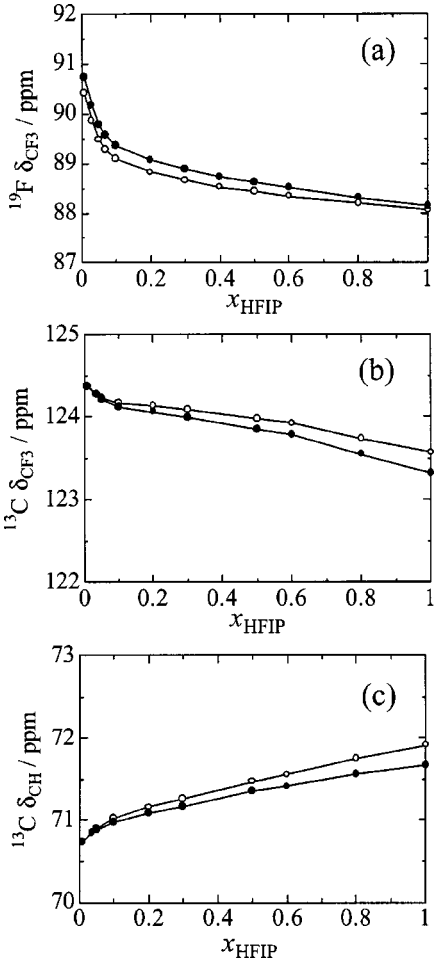

FIG. 7. ^{19}F-NMR chemical shift of HFIP CF_3 groups (a) and ^{13}C-NMR chemical shifts of HFIP CF_3 (b) and CH (c) groups as a function of x_{HFIP} for the HFIP-water mixtures at 30 °C. The raw values (○) and magnetic susceptibility-corrected ones (●).

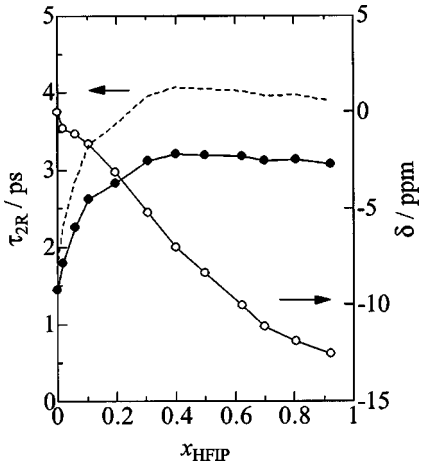

FIG. 8. ^{17}O chemical shifts, δ, and rotational correlation times, τ_{2R}, of water in the HFIP-water mixtures as a function of x_{HFIP} at 30 °C. The ^{17}O-δ values were referred to that of pure H_2O.

The ^{13}C-δ_{CF3} values shift to a lower field with decreasing x_{HFIP}, showing the deshielding of C–F carbon; the result is consistent with the tendency of ^{19}F-δ_{CF3}. An inflection point has also been observed at a similar HFIP composition as seen in ^{19}F-δ_{CF3}. Here, it is interesting to compare the present ^{13}C-δ_{CF3} values with the ^{13}C-δ_{CH3} data of the ethanol-water mixtures. The ^{13}C-δ_{CH3} data in ethanol-water mixtures also shift to a lower field with decreasing alcohol concentration, but the absolute values of the shift are much larger for ethanol-water mixtures than for HFIP-water solutions over the whole alcohol concentration range.[44] This difference can be ascribed to the large electronegativity of an F atom as discussed in Refs. 20 and 21.

The ^{13}C-δ_{CH} values show a higher field shift with decreasing x_{HFIP}. An inflection point appears at $x_{HFIP}\sim 0.08$, which is less pronounced than those for the ^{19}F-δ_{CF3} and ^{13}C-δ_{CF3} values.

The inflection points at $x_{HFIP}\sim 0.08$ for the ^{19}F-δ_{CF3}, ^{13}C-δ_{CF3}, and ^{13}C-δ_{CH} correspond well to the maximum concentration fluctuations of HFIP clusters found in the SANS study, but appear at a slightly lower x_{HFIP} than that for the LAXS data. The present NMR data confirm that the structural transition of the solvent clusters occurs at $x_{HFIP}\sim 0.08$.

D. ^{17}O-NMR chemical shift and relaxation time

Figure 8 shows the ^{17}O chemical shift of water, ^{17}O-δ_{H2O}, as a function of x_{HFIP}. With an increase in HFIP content the ^{17}O-δ_{H2O} values decrease, showing an increase in electron density of water oxygen. This result surely reflects the disruption of the hydrogen bonds of water molecules, i.e., the tetrahedral-like hydrogen-bonded water structure is gradually broken down, and the neat HFIP structure is enhanced as previously discussed. Although the ^{19}F-δ_{CF3}, ^{13}C-δ_{CF3}, and ^{1}H-δ_{CH} values of HFIP all have an inflection point at $x_{HFIP}\sim 0.08$ due to the structural transition, such an inflection point was not observed in the ^{17}O-δ_{H2O} values. This is simply because in the water-rich region the ^{17}O-δ_{H2O} values are dominated by a large amount of bulk water and

the effect of the structure-sensitive water molecules around HFIP clusters on the ^{17}O-δ_{H2O} might be difficult to detect. The structural characteristics of water in the HFIP-water mixtures can be seen in the water-poor region as an inflection point observed at $x_{HFIP}\sim 0.7$. The decreasing rate of the ^{17}O-δ_{H2O} values becomes more moderate in the region of $x_{HFIP}\geqslant\sim 0.7$, compared with that at $x_{HFIP}\leqslant 0.7$. It is known that addition of alcohol into water strengthens hydrogen bonding around the alcohol hydroxyl group as often found in molecular dynamics simulations of alcohol-water mixtures.[45] This effect tends to decrease the electron density of water oxygen or increase the ^{17}O-δ_{H2O} values. In the region of $x_{HFIP}\geqslant\sim 0.7$ only a small amount of water remains and is thus sensitive to this effect, resulting in the moderate decrease in the ^{17}O-δ_{H2O} values. The inflection point in the ^{17}O-δ_{H2O} values might suggest another structural transition at $x_{HFIP}\sim 0.7$.

The ^{17}O relaxation takes place mainly by the electric quadrupole interaction with the electric filed gradient produced by surrounding electric charges within molecules containing a ^{17}O nucleus; hence the spin-rotational and the intermolecular and intramolecular dipole–dipole contributions to the ^{17}O spin-lattice relaxation time (T_1) can be neglected. Thus, ^{17}O-T_1 of water provides information about the local motion of the water molecules. The ^{17}O-T_1 can be related to the rotational correlation time, τ_{2R}, as expressed by Eq. (7) under an extreme narrowing condition ($\omega\tau_{2R}\ll 1$: ω is the resonance frequency)[46]

$$\frac{1}{T_1}=\frac{3\pi^2}{10}\frac{2I+3}{I^2(2I-1)}\left(1+\frac{\eta^2}{3}\right)\left(\frac{e^2Qq}{h}\right)^2\tau_{2R}. \tag{7}$$

Here, e^2Qq/h is the quadrupole coupling constant (QCC), η is an asymmetric parameter, and I is the nuclear spin moment ($=5/2$ for ^{17}O). τ_{2R} is a time-averaged value of the time correlation function of the second-order orientation of the principle axis of the electric field gradient of ^{17}O, which corresponds to the direction of water dipole, and thus reflects the rotational motion of an H_2O molecule.

Figure 8 shows the ^{17}O-τ_{2R} values of water molecule obtained by using the QCC (8.9 MHz) and η(0.72) values for ^{17}O in pure water[47] for the HFIP-water mixtures against the HFIP concentration; the numerical values are given in Table III. Here, it should be borne in mind that the ^{17}O-QCC and η values might depend on the compositions of HFIP-water mixtures. To our knowledge, however, neither QCC nor η values for HFIP-water mixtures are available in the literature. For aliphatic alcohol-water mixtures of 10 mol % alcohols, the QCC values of ^{17}O were estimated from the ^1H and ^{17}O relaxation time measurements as 7.39, 7.04, and 6.64 MHz for methanol, ethanol, and 1-propanol, respectively.[48] Bagno *et al.* reported from their *ab initio* molecular orbital calculations on a number of organic solvents including aliphatic alcohols that the QCC values do not change appreciably.[49] Therefore, the different ^{17}O-QCC values found for the aqueous 10 mol % alcohol solutions probably originate from the degree of hydrogen bonding of water molecules. In the present HFIP-water mixtures, the hydrogen bonds of water molecules upon addition of HFIP lessen as found in the previous sections, and thus the ^{17}O-QCC values would be lowered with decreasing water content, though the quantitative estimation of hydrogen bonds is difficult. In the present study, thus τ_{2R} values were also calculated by using the ^{17}O-QCC (7.9 MHz) and η(0.75) values for water vapor[50] as an extreme case of least hydrogen bonding and are included in Fig. 8 (dashed line).

TABLE III. ^{17}O-NMR rotational correlation time, τ_{2R}, of H_2 ^{17}O as a function of HFIP mole fraction x_{HFIP} of the HFIP-water mixtures at 30 °C. m is the molality of H_2 ^{17}O in the respective solutions. Natural abundance of ^{17}O is 0.0204 mol kg^{-1}.

x_{HFIP}	$m(^{17}O)$/mol kg^{-1}	τ_{2R}/ps
0	0.340	1.44±0.02
0.0180	0.292	1.79±0.02
0.0605	0.213	2.26±0.03
0.106	0.368	2.62±0.03
0.196	0.278	2.83±0.04
0.304	0.206	3.12±0.04
0.400	0.165	3.21±0.04
0.498	0.239	3.19±0.04
0.623	0.158	3.17±0.04
0.699	0.108	3.12±0.04
0.806	0.0615	3.13±0.04
0.922	0.136	3.07±0.04

Apparently, the τ_{2R} values increase sharply with increasing HFIP concentration in the water-rich region ($x_{HFIP}\leqslant 0.1$), then more slowly in the region $\sim 0.1<x_{HFIP}\leqslant 0.3$ and finally become almost constant at $x_{HFIP}\gtrsim 0.3$. As seen from the dashed line for the least hydrogen bonding, the effect of the ^{17}O QCC values on τ_{2R} amounts to around a quarter of the increment in τ_{2R}. Thus, the characteristic feature in τ_{2R} does show a change in the dynamic properties of water molecules in HFIP-water molecules with HFIP mole fraction. It should be noted that the τ_{2R} values in the HFIP-water mixtures are larger than those in bulk water over the whole HFIP concentrations, i.e., the rotational motion of water molecules is retarded when HFIP is added into water. The sharp increase in τ_{2R} in the range of $0<x_{HFIP}\leqslant 0.1$ will be due to the formation of the hydration shell around the HFIP hydroxyl group. Almost constant τ_{2R} values in the region of $x_{HFIP}\gtrsim 0.3$ might be interpreted in such a way that the hydrogen bonds between water molecules are replaced with water-HFIP hydrogen bonds. This behavior in τ_{2R} in the alcohol-rich region of the HFIP-water mixtures is in marked contrast with that for dioxane-water mixtures.[41] In aqueous mixtures of dioxane the rotation of water molecules is accelerated in a dioxane-rich region because the water–water hydrogen bonds are disrupted by aprotic dioxane molecules to generate more monomeric water molecules.[41]

It should be commented that a similar inflection point has been found at $x_{HFIP}\sim 0.2$ in the rotational correlation time, τ_c, of $^{13}C(CF_3)$ in an NMR study of HFIP-water mixtures.[21] From the present and the literature[21] results the inflection point in the dynamic properties appear at a slightly higher HFIP concentrations than that for the SANS measurements.

To investigate the nature of the hydration shell of HFIP in water, the NMR B coefficient[31] was calculated. In the very

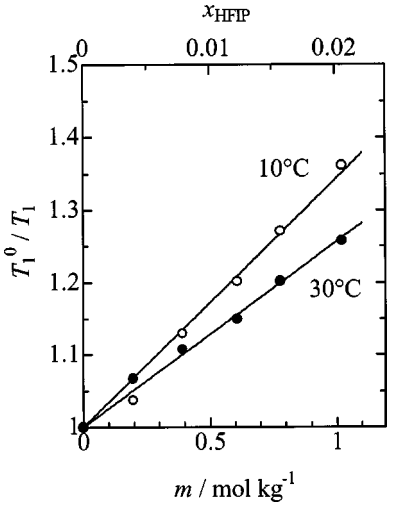

FIG. 9. Ratios T_1^0/T_1 of ^{17}O spin-lattice relaxation times in bulk and in the HFIP-water mixtures as a function of HFIP molality m and mole fraction, x_{HFIP}, at 10 °C (○) and 30 °C (●).

dilute concentration range of aqueous HFIP solutions in which the HFIP-HFIP interaction is negligible, a ratio of ^{17}O-T_1 in bulk water and in HFIP-water mixtures, T_1^0/T_1, can be expressed as a function of molality m of HFIP as

$$\frac{T_1^0}{T_1} = 1 + Bm. \tag{8}$$

When water molecules are strongly bound to a solute, such as for ionic hydration, the rotation of water molecules is hindered to make the B coefficient less temperature-dependent. On the other hand, when the hydrogen-bonded network is strengthened, e.g., by lowering the temperature, the B coefficient increases at the lower temperatures. Figure 9 shows the concentration dependence of the T_1^0/T_1 ratios of the HFIP concentrations below 1 mol/kg ($x_{HFIP}=0.02$). The linearity between T_1^0/T_1 and m was obtained within experimental errors. The B coefficients of HFIP at 10 and 30 °C obtained from the slope are given as a function of HFIP molality in Table IV. The B coefficients at 10 and 30 °C are both positive and decrease with increasing temperature. This finding suggests enhancement of the water structure in the hydration shell around HFIP, which is consistent with the LAXS, SANS, and MD results.

TABLE IV. ^{17}O-T_1 values of $H_2{}^{17}O$ in the HFIP-water mixtures as a function of HFIP molality and mole fraction x_{HFIP}, and the B coefficients of HFIP at 10 and 30 °C.

		T_1 /ms	
m (mol kg^{-1})	x_{HFIP}	10 °C	30 °C
0	0	4.18±0.05	7.62±0.08
0.197	0.003 94	4.03±0.06	7.14±0.15
0.391	0.007 82	3.70±0.04	6.88±0.10
0.607	0.0121	3.48±0.03	6.63±0.05
0.778	0.0156	3.29±0.04	6.34±0.05
1.02	0.0204	3.07±0.06	6.06±0.10
B (kg^{-1} mol)		0.34±0.02	0.26±0.01

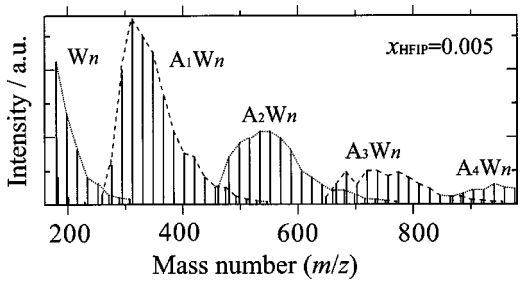

FIG. 10. Typical mass spectrum of the clusters isolated from liquid droplets of the HFIP-water mixture at $x_{HFIP}=0.005$. A_mW_n and W_n stand for $H^+(HFIP)_m(H_2O)_n$ and $H^+(H_2O)_n$, respectively. Hydration sequences of HFIP m-mer hydrates and water n-mer clusters are shown with broken and dotted lines.

E. Mass spectrometry

The ionization of HFIP-water binary clusters can be described as dissociation processes producing free water (W) or free HFIP (A) and an OH radical:

$$A_mW_n + e^- \rightarrow H^+A_mW_{n'} + \mathrm{OH} + (n-n'-1)W + 2e^-$$

or

$$\rightarrow H^+A_{m'}W_n + \mathrm{OH} + (m-m'-1)A + 2e^-$$

$$W_n + e^- \rightarrow H^+W_{n'} + \mathrm{OH} + (n-n'-1)W + 2e^-.$$

Hereafter, binary ions of HFIP m-mer hydrates $H^+A_mW_n$ are abbreviated as A_mW_n, while protonated water clusters H^+W_n as W_n.

Figure 10 shows a typical mass spectrum of the HFIP-water mixture at $x_{HFIP}=0.005$. Hydration sequences of the A_mW_n and W_n are shown with broken and dotted lines. It should be noted that a previous study on ethanol-water mixtures demonstrated that spectral patterns do not change on varying the electron impact energies from 20 to 40 eV. In Fig. 10 are plotted clusters whose mass numbers fall in the range of 200 to 1000, since those with the mass number less than 200 are small clusters, such as monomer, dimer, and trimer, whereas large clusters with the mass number greater than 1000 are formed less often.

Figure 11 shows the distribution of the A_mW_n and W_n found as a function of the number of water molecules in them at the various x_{HFIP}. As seen in Fig. 11, the hydration numbers of the clusters decrease with increasing x_{HFIP}, particularly at concentrations higher than $x_{HFIP}=0.09$. At the higher concentrations the average hydration numbers were less than 6 for $m=1$ to 3, while those at $x_{HFIP}=0.005$ and 0.01 were 10 for $m=1$ and 16 for $m=4$. Apparently, the hydration structure is highly disrupted at the high concentrations. Another striking feature in the spectra is that the intensities of the HFIP monomer hydrates are much larger than those of the oligomer hydrates at $x_{HFIP}=0.09$ and 0.2. The oligomer hydrates with $m=2$, 3, and 4 appear to be stabilized only when sufficient numbers of water molecules are available to hydrate HFIP molecules. This result implies that clustering of HFIP molecules is preferred in a water-rich region as found in the present LAXS, SANS, and NMR measurements.

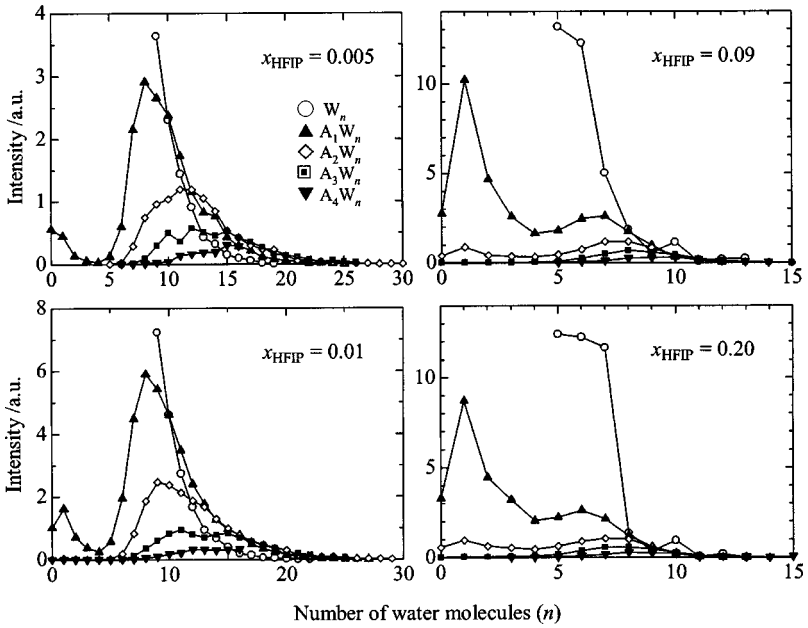

FIG. 11. Distributions of water clusters (W_n) and HFIP-water clusters (A_mW_n) vs number of water molecules (n) in them obtained from the mass spectra for the HFIP-water liquid droplets at various HFIP mole fractions, x_{HFIP}.

The present mass spectral result on the formation of oligomers of the HFIP-water mixtures is in marked contrast with those of aqueous mixtures of aliphatic alcohols, such as methanol[13] and ethanol,[14–16] in which the higher the concentrations of the aliphatic alcohols, the larger the oligomers. This difference should be ascribed to the degree of hydrogen bonding between alcohols; as evidenced in the DRDFs of the LAXS data, the hydrogen bonds between HFIP molecules would be too weak to form stable oligomers by the adiabatic expansion process.

IV. CONCLUSION

The structure and dynamic properties of HFIP-water binary solutions have been revealed at a molecular level as a function of alcohol concentration by LAXS, SANS, ^{19}F-, ^{13}C-, and ^{17}O-NMR chemical shifts and ^{17}O-NMR relaxation, and mass spectrometry. The LAXS, SANS, and NMR data have all shown the structural transition of clusters at x_{HFIP} 0.06–0.1. The x-ray RDFs have demonstrated the structural transition from tetrahedral-like water clusters in the range of $x_{HFIP} \leqslant 0.1$ to the intrinsic structure of HFIP in the range of $x_{HFIP} \geqslant 0.15$. The SANS data have shown that clustering or microhetrogeneities of HFIP-water mixtures has a maximum at $x_{HFIP} \sim 0.06$ with a correlation length of 9.7 Å. The NMR data have suggested such structure of the clusters as the hydrophobic CF_3 groups aggregate as an inside core and the hydrophilic OH groups outside to form hydrogen bonds with surrounding water molecules. The NMR relaxation data of water in HFIP-water solutions have shown that the rotational motion of water molecules are retarded upon addition of HFIP into water with the structural transition taking place at a similar HFIP concentrations as found in the LAXS measurements. The mass spectra have revealed that HFIP oligomers A_mW_n $(m=2-4)$ are formed only in the water-rich region of $x_{HFIP} \leqslant 0.01$ and that monomeric HFIP water clusters A_1W_n $(n=5-20)$ are stabilized in the region of $x_{HFIP} \geqslant 0.09$. These results of the mass spectra are consistent with the clustering in HFIP molecules in a water-rich region of bulk HFIP-water mixtures.

ACKNOWLEDGMENTS

This work was supported in part by the Joint Studies Program (1998) of the Institute for Molecular Science. The authors gratefully thank Dr. Y. Sakamoto of Institute for Molecular Science for ^{19}F-NMR measurements, and Professor K. Mizuno and Y. Tamiya for discussion about the magnetic susceptibility correction for NMR spectra. The authors thank Dr. A. Barnes of the University of Bristol for checking the English.

[1] M. Barteri, M. C. Gaudiano, G. Mei, and N. Rosato, Biochim. Biophys. Acta **1383**, 317 (1998).
[2] A. Kentsis and T. R. Sosnick, Biochemistry **37**, 14613 (1998).
[3] V. Bhakuni, Arch. Biochem. Biophys. **357**, 274 (1998).
[4] C. Ruckerbusch, N. Nedjar-Arroume, S. Magazazeni, J.-P. Huvenne, and P. Legrand, J. Mol. Struct. **478**, 185 (1999).
[5] S. Cinelli, G. Onori, and A. Santucci, Colloids Surf., B **160**, 3 (1999).
[6] R. Rajan and P. Balaram, Int. J. Pept. Protein Res. **48**, 328 (1996).
[7] M. Buck, H. Schwalbe, and C. M. Dobson, J. Mol. Biol. **257**, 669 (1996).
[8] H. Lu, M. Buck, S. E. Radford, and C. M. Dobson, J. Mol. Biol. **265**, 112 (1997).
[9] S. Kumaran and R. P. Roy, J. Pept. Res. **53**, 284 (1999).
[10] F. Khan, R. H. Khan, and S. Muzammil, Biochim. Biophys. Acta **1481**, 229 (2000).
[11] R. Stoll, W. Voelter, and T. A. Holak, Biopolymers **41**, 623 (1997).
[12] N. Hirota-Nakaoka and Y. Goto, Bioorg. Med. Chem. **7**, 67 (1999).
[13] T. Takamuku, T. Yamaguchi, M. Asato, M. Matsumoto, and N. Nishi, Z. Naturforsch. A **55**, 513 (2000).
[14] M. Matsumoto, N. Nishi, T. Furusawa, M. Saita, T. Takamuku, M. Yamagami, and T. Yamaguchi, Bull. Chem. Soc. Jpn. **68**, 1775 (1995).
[15] N. Nishi, S. Takahashi, M. Matsumoto, A. Tanaka, K. Muraya, T. Takamuku, and T. Yamaguchi, J. Phys. Chem. **99**, 462 (1995).
[16] N. Nishi, M. Matsumoto, S. Takahashi, T. Takamuku, M. Yamagami, and T. Yamaguchi, Proc. Yamada Conf. XLIII, 113 (1996).
[17] D. T. Bowron, J. L. Finney, and A. K. Soper, J. Phys. Chem. B **102**, 3551 (1998).
[18] T. Yamaguchi, Pure Appl. Chem. **71**, 1741 (1999).
[19] W. Y. Wen and J. A. Muccitelli, J. Solution Chem. **8**, 25 (1979).
[20] K. Kinugawa and K. Nakanishi, J. Chem. Phys. **89**, 5834 (1988).

[21] Y. Mizutani, K. Kamogawa, T. Kitagawa, A. Shimizu, Y. Taniguchi, and K. Nakanishi, J. Phys. Chem. **95**, 1790 (1991).
[22] M. Fioroni, K. Burger, A. E. Mark, and D. Roccatano, J. Phys. Chem. B **105**, 10967 (2001).
[23] D. Hong, M. Hoshino, R. Kuboi, and Y. Goto, J. Am. Chem. Soc. **121**, 8427 (1999).
[24] K. Yamanaka, T. Yamaguchi, and H. Wakita, J. Chem. Phys. **101**, 9830 (1994).
[25] T. Yamaguchi, H. Wakita, and K. Yamanaka, Fukuoka Univ. Sci. Rep. **29**, 127 (1999).
[26] G. Johansson and M. Sandström, Chem. Scr. **4**, 195 (1973).
[27] K. Furukawa, Rep. Prog. Phys. **25**, 395 (1962).
[28] J. Krogh-Moe, Acta Crystallogr. **2**, 951 (1956).
[29] N. Norman, Acta Crystallogr. **10**, 370 (1957).
[30] D. T. Cromer and J. B. Mann, J. Chem. Phys. **47**, 1892 (1967).
[31] J. A. Ibers, D. H. Templeton, B. K. Vainshtein, G. E. Bacon, and K. Lonsdale, *International Tables for X-Ray Crystallography*, edited by K. Lonsdale, Vol. 3, Sec. 3, 201 (Kynoch, Birmingham, 1962).
[32] V. F. Sears, Neutron News **3**, 26 (1992).
[33] K. Mizuno, S. Imafuji, T. Ochi, T. Ohta, and S. Maeda, J. Phys. Chem. B **104**, 11001 (2000).
[34] K. Momoki and Y. Fukuzawa, Anal. Chem. **62**, 1665 (1990).
[35] K. Momoki and Y. Fukuzawa, Anal. Sci. **10**, 53 (1994).
[36] F. Fister and H. G. Hertz, Ber. Bunsenges. Phys. Chem. **71**, 1032 (1967).
[37] N. Nishi, K. Koga, C. Oshima, K. Yamamoto, U. Nagashima, and K. Nagami, J. Am. Chem. Soc. **110**, 5246 (1988).
[38] N. Nishi, Z. Phys. D: At., Mol. Clusters **15**, 239 (1990).
[39] N. Nishi and K. Yamamoto, J. Am. Chem. Soc. **109**, 7353 (1987).
[40] K. Yamamoto and N. Nishi, J. Am. Chem. Soc. **112**, 549 (1990).
[41] T. Takamuku, A. Yamaguchi, M. Tabata, N. Nishi, K. Yoshida, H. Wakita, and T. Yamaguchi, J. Mol. Liq. **83**, 163 (1999).
[42] H. E. Stanley, *Introduction to Phase Transitions and Critical Phenomena* (Clarendon, Oxford, 1971).
[43] G. D'Arrigo and J. Teixeira, J. Chem. Soc., Faraday Trans. **86**, 1503 (1990).
[44] K. Mizuno, K. Oda, S. Maeda, and Y. Shindo, J. Phys. Chem. **99**, 3056 (1995).
[45] P. G. Kusalik, A. P. Lyubartsev, D. L. Bergman, and A. Laaksonen, J. Phys. Chem. B **104**, 9526 (2000).
[46] A. Abragam, *The Principles of Nuclear Magnetism* (Oxford, London, 1963), p. 313.
[47] R. Eggenberger, S. Gerber, H. Huber, D. Searles, and M. Welker, Mol. Phys. **80**, 1177 (1993).
[48] R. Ludwig, Chem. Phys. **195**, 329 (1995).
[49] A. Bagno, G. Lovato, G. Scorrano, and W. J. Wijinen, J. Phys. Chem. **97**, 4601 (1993).
[50] R. P. W. J. Struis, J. de Bleijser, and J. C. Leyte, J. Phys. Chem. **91**, 1639 (1987).